Cerous Fluoride Dopant-Free Electron-selective Contact for Crystalline Silicon Solar Cells

Wenxian Wang, Lun Cai, Lanxiang Meng, LinKun Zhang, Nuo Chen, Hui Shen, and Zongcun Liang *

X. Wang, Dr. L. Cai, L. Meng, L. Zhang, N. Chen, Prof. H. Shen,
Prof. Z. Liang
Institute for Solar Energy Systems
Guangdong Provincial Key Laboratory of Photovoltaic Technology
School of Physics
Sun Yat-Sen University
Guangzhou 510006, P.R. China
E-mail: liangzc@mail.sysu.edu.cn
Dr. L. Cai,
School of Materials
Sun Yat-Sen University
Shenzhen 518107, P.R. China

Keywords

Cerous Fluoride, dopant-free, electron-selective contact, silicon solar cells, passivated contact, contact resistivity

Abstract

Dopant free carrier-selective contacts have drawn intensive attention for efficient crystalline silicon (c-Si) photovoltaics due to low-temperature simple process and better carrier selectivity. By incorporating a thermal-evaporated dielectric film cerium fluoride (CeF_3) as the electron transport layer (ETL) between c-Si(n) and aluminum(Al) electrode,

higher conversion efficiency of the crystalline silicon solar cell is present, which is 21.27% compared to 16.89% of reference cell without CeF_3. The insertion of an ultrathin CeF_3 ETL help alleviating the strong fermi-level pinning at the interface and leading to better electron transport with a low contact resistivity of 10.96 $m\Omega \cdot cm^2$. The morphology and element distribution of the interface were also investigated by high resolution transmission electron microscopy (HRTEM). Our primary results demonstrate that the utilization of kinds of lanthanide fluorides including CeF_3 offering a good choice for efficient and cost-effective electron selective contact for optical-electrical devices.

1 Introduction

Crystalline silicon (c-Si) has dominated worldwide photovoltaic (PV) market for many years. The traditional silicon solar cells are mostly based on p-type silicon wafers with a front phosphorus diffusion region as electron selective contact and a heavily aluminum (Al) doped region on the rear surface as hole selective contact.[1] These carrier selective contacts formed by high-temperature-diffusion results in serious Auger recombination and SRH recombination underneath the metal electrodes.[2-4] To overcome this shortage, it is necessary to insert a buffer layer between metal and c-Si. This could also solve the problem of strong fermi level pining at the metal-semiconductor interface, which will impede carrier selective transport.[5,6] A successful application of this strategy is silicon solar cells based on Heterojunction with Intrinsic Thin-layer (HIT), which demonstrates a very high efficiency up to 26.7%.[7] However, this type hetero-contact also involves doping very thin amorphous silicon films. Precisely doping of thin films adds the process complexity and cost. Furthermore, the doped thin films also introduce serious parasitic optical absorption due to their narrow bandgap and increased free-carrier absorption.[8]

Dopant-free carrier selective contacts afford a better routine. Some thin films such as MoO_3,[9-12] WO_3,[13,14] Cs_2CO_3,[15] LiF,[5,16] MgF_2,[17,18] MgO_x,[6] $Mg(Acac)_2$,[19] etc. have larger bandgap and proper work-function without artificial doping. By just simple evaporation or spin-coating onto n-Si, excellent carrier selectivity and high efficiency could be achieved with these materials. Thus, the dopant-free carrier selective contacts could significantly decrease the cost of efficient silicon solar cells.

Alkali earth metal compounds are often used as electron injection/extraction layer in organic cells, OLED and photoelectric detectors. The potential of rare earth metal compounds working as efficient dopant-free electron selective contact for silicon solar cells has never been investigated before. Cerium is the most abundant rare-earth metal in the Earth's crust.[20,21] Besides, the chemical activity of cerium is similar to that of alkaline earth metals. In this paper, thin CeF_3 film was deposited by thermal evaporation at room temperature. No decomposition of CeF_3 was found as confirmed by X-ray photoelectron spectroscopy (XPS). And it is found that the insertion of thin CeF_3 alleviates the strong fermi-level pinning at the interface and leading to better electron transport with a low contact resistivity of 10.96 $m\Omega \cdot cm^2$ for an optimized thickness of 1.5 nm. The morphology and element distribution of the interface were also investigated by high resolution transmission electron microscopy (HRTEM). The application of CeF_3/Al to a n-type PERC solar cell has demonstrates a champion efficiency of 21.27%, while the one without CeF_3 show rather poor efficiency of 16.89%. Our primary results demonstrate that the utilization of kinds of lanthanide compounds including CeF_3 offering a good choice for efficient electron selective contact for optical-electrical devices with low-cost.

2 Experimental Section

2.1. Materials and Contact Characterization. N-type (100)-oriented C-z silicon wafers (≈180 μm) with a resistivity of 1-3 Ω·cm were used as substrates for all the samples and solar cells fabrication. CeF_3 thin films were thermally evaporated at a rate of 0.1 Å/s from high purity (99.99%) CeF_3 powder. The base pressure in the evaporation chambers was under 8 ×

10^{-4} Pa. The structure of CeF_3 pure powder and thin films were characterized with X-ray diffraction (XRD). Thicker (≈100 nm) CeF_3 films deposited on polished wafers were characterized by a PANalytical X'Pert PRO MRD diffractometer with Cu Kα radiation (λ = 0.154 nm) at 40 kV. XRD data were analyzed by the software MDI Jade.

For X-ray photoelectron spectroscopy (XPS) and ultraviolet photoelectron spectroscopy (UPS) characterization, all of the samples were fabricated on polished c-Si(n) wafers. A Thermo Scientific ESCALAB 250Xi spectrometer with a monochromatic Al Kα x-ray source (hv = 1486.6 eV) and He I source (hv = 21.22 eV) are used for the measurements. A bias voltage of -5V was added to the samples to obtain its secondary electron cutoffs. High-resolution transmission electron microscope (HRTEM) cross-section images of the c-Si/SiO_x/CeF_3/Al rear contact layer were observed by using a TEM (JEM-2100F, 200 kV, JEOL corporation) in a combination of energy-dispersive X-ray spectroscopy (EDX) line scanning. The contact resistivity between c-Si and variety thickness of CeF_3 thin films were extracted by a transfer-length-method (TLM) and tested in dark environment using a Keithley 2400 source meter.

2.2. Cell Fabrication and Characterization. Proof-of-concept 2 × 2 cm^2 n-type cells were fabricated on the same wafers mentioned above. After texturing to form an array of random pyramids in KOH solution and the Radio Corporation of America (RCA) cleaning, a p-type emitter was thermally diffused via a born furnace. Then the front boron emitter and back surfaces were passivated with Al_2O_3/SiN_x stack layers deposited by Atomic layer deposition (ALD) and plasma-enhanced chemical vapor deposition (PECVD), respectively. A

picosecond laser was used to open 25 μm-diameter holes on the rear back surfaces to facilitate electrode contact. The front Ag grid contacts were fabricated by screen-printing paste and firing. The solar cells were completed by covering the undiffused rear surfaces by different stacks, such as direct Al, and CeF_3/Al. The current-voltage (*J-V*) measurements were conducted under simulated AM1.5G illumination (100 mW cm^{-2}, 25 °C) using a calibrated WPVS reference cell. The external quantum efficiency (EQE) measurements were carried out by a spectrum corresponding QE-R spectra test system from Enli-tech.

3 Results and Discussion

The morphology of CeF_x thin films are continuous as characterized by atomic force microscopy (AFM), showing a surface roughness R_a of only 0.378 nm (shown in Figure S1). To scrutinize the structure of embedded CeF_3, the XRD analysis of grown crystal was performed compared with the CeF_3 pure powder, as shown in Figure S2. Diffraction peaks at 2θ as 25, 28, 35, 44, 45, 51, 53 and 65° are corresponded to space indexes of (110), (111), (112), (300), (113), (302), (310) and (222), respectively, which are in agreement with CeF_3 hexagonal crystal (PDF# 70-0002).[22]

The atomic composition and chemical states of Ce, F in CeF_x was obtained by the X-ray photoelectron spectroscopy (XPS) characterization. As it is illustrated in **Figure 1**. The binding energies of all peaks were recalibrated by the surface pollution C 1s at 284.8 eV. The F 1s spectra exhibits the main peak at 684.9 eV as is shown in **Figure 1**a. **Figure 1**b shows the core level of the Ce spectrum can be recognized into four peaks. Two Ce $3d_{5/2}$ predominant peaks at 884.2 eV and 887.7 eV binding energy, and Ce $3d_{3/2}$ spectrum was

ascribed to the two binding energies of 902.5 eV and 906.0 eV, respectively. In addition, there is a weak satellite peak at higher binding energy, which is in well agreement with those previous articles for CeF_3 thin films.[23,24] The F to Ce atom ratio extracted from the core level peak areas confirms the obtained thin film is stoichiometric CeF_3.

Figure 1c-d shows the ultraviolet photoelectron spectroscopy (UPS) measurement results. The work function of CeF_x as indicated in the secondary electron cut-off vicinity is 3.16 eV, which is the main reason for the fine Ohmic contact on c-Si(n). The maximum valence band edge (E_{VBM}) located 4.5 eV below the fermi-level (E_F). The band gap of CeF_3 is about 4.9 eV as commonly reported in literatures.[25,26] It is easy to calculate that the electron affinity is 2.76 eV and the fermi level lays 0.4 eV below the conduction band, which means the obtained CeF_3 film is n-type and is favorable for electron transport from conduction band or by tunneling. The low work function of CeF_x layer allow for good electron transport from n-Si and the huge valence band offset between CeF_x and c-Si(n), blocked holes transport.

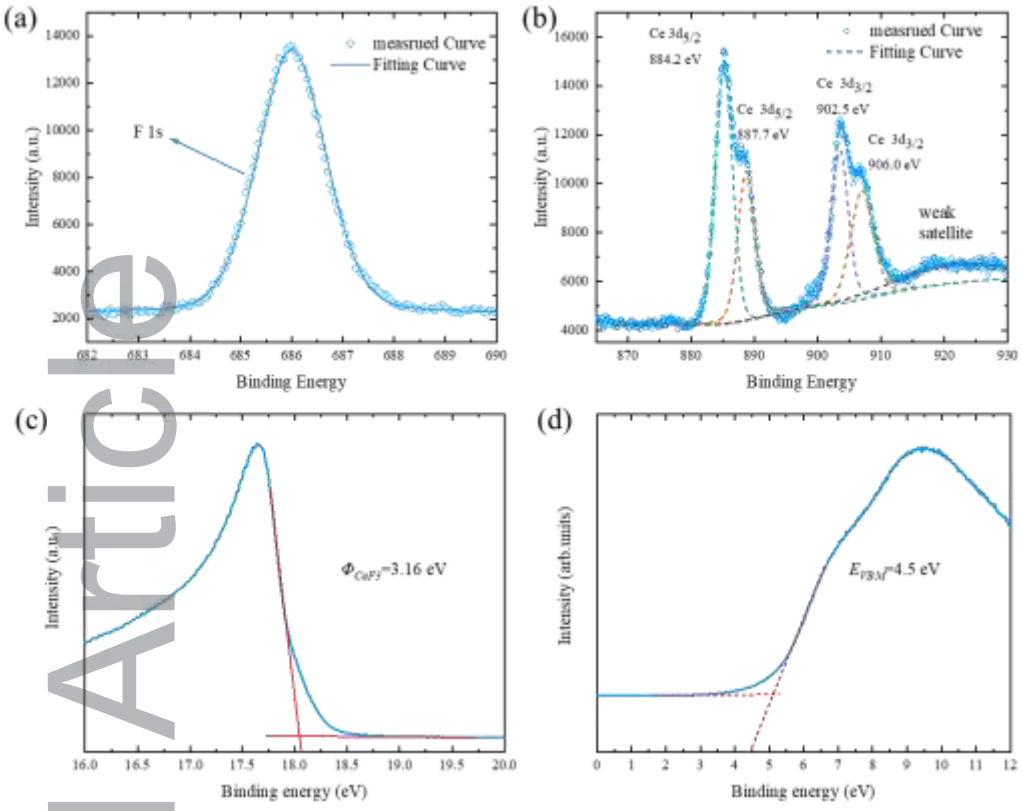

Figure 1. XPS and UPS measurements of thermally evaporated CeF_x film. a) The core level spectrum of F 1s. b) Core spectrum of Ce 3d. c) Work function of CeF_x extracted from the secondary electron cut-off spectrum. c) Valence band spectrum of the CeF_x film.

Low contact resistivity is an indispensable condition to form high electron selectivity. To evaluate the contact resistivity (ρ_c) of the CeF_3/c-Si(n)/Al stack, the transfer length method (TLM) is employed and the measurement results are shown in **Figure 2**. It is well known that Al forms rectifying contact to lightly doped n-Si (1–10 Ω·cm) due to the large Schottky barrier height (Φ > 0.7 eV), which is a consequence of strong Fermi-level pinning effect.[27] By contrast, with the insertion of a CeF_3 thin film between c-Si and Al， the contact behavior converted into an Ohmic contact. The contact resistivity ρ_c is 10.96 mΩ·cm^2 for the 1.5 nm CeF_3/Al stack as shown in **Figure 2**a, which is significantly lower than the contact of Al/n-Si(~2 Ω·cm^2).[28] When the thickness of CeF_3 increases, ρ_c increases but the contact

remains Ohmic (ρ_c = 82 mΩ·cm^2). The variation of ρ_c with different film thickness is shown in **Figure 2**b.

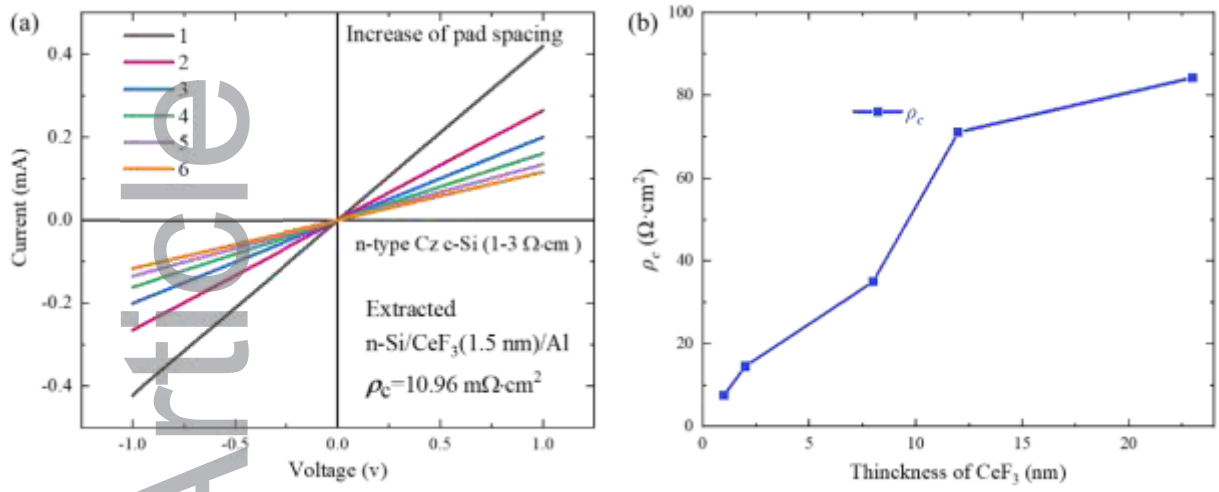

Figure 2. Contact resistivity measurements of CeF_3/Al contacts to n-Si using TLM. a) Dark I–V measurement result of CeF_3(1.5 nm)/Al stack layer on 1-3 Ω·cm c-Si(n). b) Contact resistivity ρ_c as a function of CeF_3 thickness.

The passivation property of CeF_3 on Cz n-Si with double-side symmetrical structure was investigated. However, no iVoc increase has been observed after the deposit of 1-5 nm CeF_3. This is similar to that of thermal evaporated MgF_2 and LiF, [18,5] which could be explained by lacking of strong bonding by this deposit method.

The scanning transmission electron microscopy (STEM) measurement combing with energy-dispersive X-ray spectroscopy (EDX) was performed to investigate the structure and composition of the c-Si/SiO_x/CeF_3 (1.5 nm)/Al interfaces. As shown in **Figure 3**a, the SiO_x and CeF_x thin-film separate the silicon from the Al layer, showing that the 1.5 nm thermally evaporated CeF_3 layer is uniform and continuous. The 0.8~1 nm SiO_x layer is typically formed by native oxidation during the process of the sample transfer and long-time vacuuming before thermal evaporation.[29,30] Synchronously, EDX maps of the CeF_3/Al/c-Si(n)

contact with a 10 nm resolution are displayed in **Figure 3**b. The Al, Ce, F, O, and Si elemental signals confirmed the presence of the CeF_x and SiO_x layers.

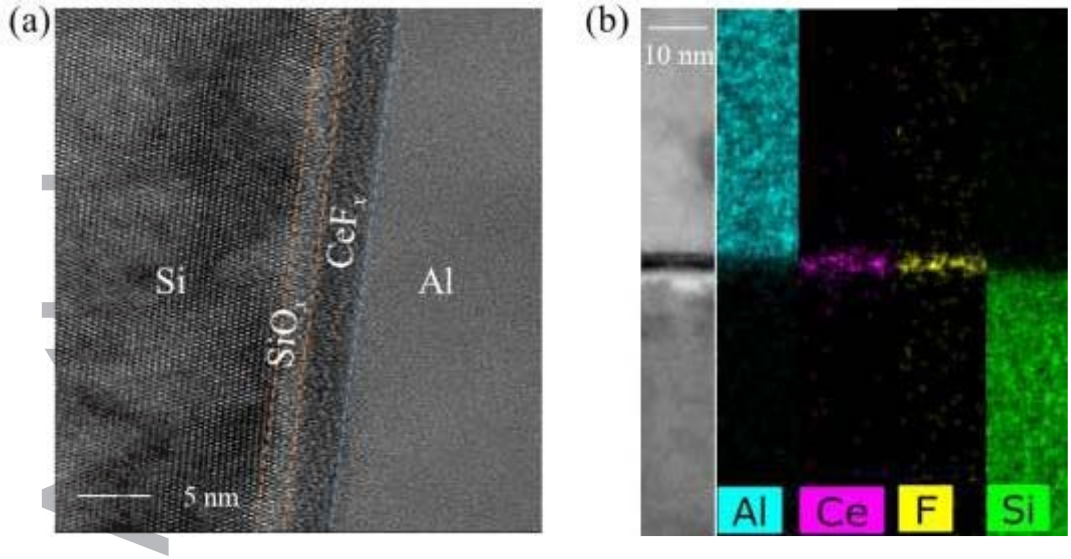

Figure 3. STEM HAADF microscopy images of CeF_3/Al (1.5 nm)/SiO_x (1 nm)/c-Si(n) contact interface. a) High-resolution STEM HAADF microscopy image of the c-Si/CeF_x/Al/ contact. b) EDX mapping of Al, Ce, F, and Si signals at 10 nm resolution.

A proof-of-concept solar cell with partial-rear CeF_3/Al contact was successfully fabricated. **Figure 4**a shows the current density–voltage (*J–V*) curves of solar cells with and without CeF_x inserted layer. The parameters of both cells are also tabulated in the image. The interlayer of a 1.5 nm thick CeF_3 film dramatically improves the cell performance, enabling a power conversion efficiency η, open-circuit voltage (V_{oc}), and short-circuit current (J_{sc}) of 21.27%, 646 mV, and 41.60 mA·cm^{-2}, respectively. The fill factor (*FF*) with the adding layer CeF_x was enhanced from 65.78% to 79.13%, demonstrating its excellent carrier selectivity. Compared to the reference cell (without CeF_3 interlayer), *FF* increased by 13.15% as result of low ρ_c compared to the reference one. Both J_{sc} and V_{oc} were slightly improved (from 40.72 mA·cm^{-2},625 mV to 41.60 mA·cm^{-2}, 646 mV). The EQE and reflection of both solar cells are

presented in **Figure 4**b. All these measurements were taken between the Ag grid fingers. Apparently, the low work function CeF_3 interlayer significantly enhances the spectral response at long wavelengths between 700 nm and 1190 nm, leading to the integration J_{sc} of the EQE improvement from 40.81 mA·cm^{-2} to 41.80 mA·cm^{-2}. The results are in line with measured J_{sc} values derived from the previous $J-V$ measurements. The internal quantum efficiency (IQE) at longer (900-1200 nm) wavelength range can indicate the contact quality of rear side. Obviously, even the CeF_3/Al cell has slightly higher reflectance at this region, its IQE is still much high than that of directly Al contact reference cell. These results proved that the applied low work function CeF_x/Al contacts provide good electron selectivity.

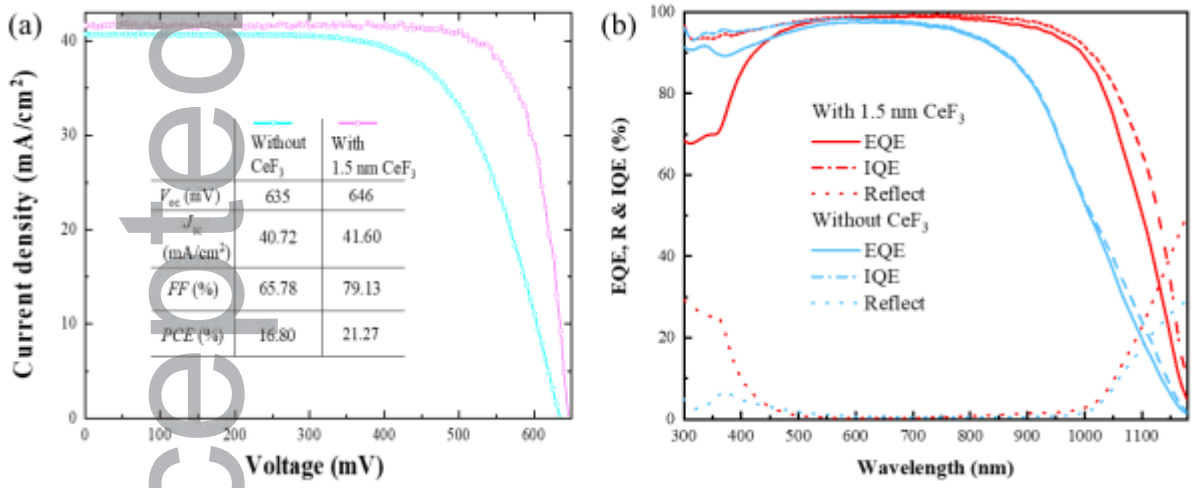

Figure 4. Device performance with and without partial rear CeF_3/Al contacts. a) Light J–V characteristics under AM1.5 conditions. b) EQE, reflectance and IQE of the cells.

4 Conclusions

The potential of rare earth metal compounds of CeF_3 thin film working as efficient dopant-free electron selective contact for silicon solar cells has been investigated for the first time. The insertion of thin CeF_3 alleviates the strong fermi-level pinning at the interface and

leading to better electron transport with a low contact resistivity of 10.96 $m\Omega \cdot cm^2$ for an optimized thickness of 1.5 nm. The application of CeF_3/Al contact to a n-type PERC solar cell has demonstrates a champion efficiency of 21.27% at moment. Our primary results point out a good choice for efficient electron selective contact for many other optical-electrical devices with low-cost.

Acknowledgements

This work was supported by the National Natural Science Foundation of China (Grant No. 61774173).

Conflict of Interest

The authors declare no conflict of interest.

References

[1] F. Fertig, R. Lantzsch, A. Mohr, M. Schaper, M. Bartzsch, D. Wissen, F. Kersten, A. Mette, S. Peters, A. Eidner, J. Cieslak, K. Duncker, M. Junghänel, E. Jarzembowski, M. Kauert, B. Faulwetter-Quandt, D. Meißner, B. Reiche, S. Geißler, S. Hörnlein, C. Klenke, L. Niebergall, A. Schönmann, A. Weihrauch, F. Stenzel, A. Hofmann, T. Rudolph, A. Schwabedissen, M. Gundermann, M. Fischer, J. W. Müller, D. J. W. Jeong, *Energy Procedia*. **2017**, *124*, 338.

[2] A. Cuevas, P. A. Basore, G. Giroult‐Matlakowski, C. Dubois, *Journal of Applied Physics*. **1996**, *80*, 3370.

[3] D. Yan, A. Cuevas, *Journal of Applied Physics*. **2014**, *116*, 194505.

[4] T. G. Allen, J. Bullock, Q. Jeangros, C. Samundsett, Y. Wan, J. Cui, A. Hessler-Wyser, S. De Wolf, A. Javey, A. Cuevas, *Advanced Energy Materials*. **2017**, *7*, 1602606.

[5] J. Bullock, P. T. Zheng, Q. Jeangros, M. Tosun, M. Hettick, C. M. Sutter-Fella, Y. Wan,

T. Allen, D. Yan, D. Macdonald, S. De Wolf, A. Hessler-Wyser, A. Cuevas, A. Javey, *Advanced Energy Materials*. **2016**, *6*.1600241.

[6] Y. M. Wan, C. Samundsett, J. Bullock, M. Hettick, T. Allen, D. Yan, J. Peng, Y. L. Wu, J. Cui, A. Javey, A. Cuevas, *Advanced Energy Materials*. **2017**, *7*.1601863.

[7] K. Yoshikawa, W. Yoshida, T. Irie, H. Kawasaki, K. Konishi, H. Ishibashi, T. Asatani, D. Adachi, M. Kanematsu, H. Uzu, K. Yamamoto, *Solar Energy Materials and Solar Cells*. **2017**, *173*.17032.

[8] Z. C. Holman, A. Descoeudres, L. Barraud, F. Z. Fernandez, J. P. Seif, S. De Wolf, C. Ballif, *Ieee Journal of Photovoltaics*. **2012**, *2*.7.

[9] M. Bivour, J. Temmler, H. Steinkemper, M. Hermle, *Solar Energy Materials and Solar Cells*. **2015**, *142*.34.

[10] B. Macco, M. F. J. Vos, N. F. W. Thissen, A. A. Bol, W. M. M. Kessels, *Physica Status Solidi-Rapid Research Letters*. **2015**, *9*.393.

[11] C. Battaglia, X. Yin, M. Zheng, I. D. Sharp, T. Chen, S. Mcdonnell, A. Azcatl, C. Carraro, B. Ma, R. Maboudian, R. M. Wallace, A. Javey, *Nano Lett*. **2014**, *14*.967.

[12] J. Bullock, A. Cuevas, T. Allen, C. Battaglia, *Applied Physics Letters*. **2014**, *105*, 232109.

[13] M. Mews, L. Korte, B. Rech, *Solar Energy Materials and Solar Cells*. **2016**, *158*.77.

[14] M. Mews, A. Lemaire, L. Korte, *Ieee Journal of Photovoltaics*. **2017**, *7*.1209.

[15] Y. Zhang, W. Cui, Y. Zhu, F. Zu, L. Liao, S.-T. Lee, B. Sun, *Energy & Environmental Science*. **2015**, *8*, 297.

[16] J. Bullock, M. Hettick, J. Geissbuhler, A. J. Ong, T. Allen, C. M. Sutter-Fella, T. Chen, H. Ota, E. W. Schaler, S. De Wolf, C. Ballif, A. Cuevas, A. Javey, *Nature Energy*. **2016**, *1*.15031.

[17] W. Wu, W. Lin, S. Zhong, B. Paviet-Salomon, M. Despeisse, Q. Jeangros, Z. Liang, M. Boccard, H. Shen, C. Ballif, *physica status solidi (RRL) – Rapid Research Letters*. **2020**, *14*, 1900688.

[18] Y. Wan, C. Samundsett, J. Bullock, T. Allen, M. Hettick, D. Yan, P. Zheng, X. Zhang, J.

Cui, J. Mckeon, A. Javey, A. Cuevas, *ACS Appl Mater Interfaces*. **2016**, *8*.14671.

[19] Z. R. Yao, L. Cai, L. X. Meng, K. F. Qiu, W. J. Lin, J. S. Jin, W. Y. Duan, K. N. Ding, S. H. Li, B. Ai, Z. C. Liang, H. Shen, *Physica Status Solidi-Rapid Research Letters*. **2020**, *14*. 2000103.

[20] X. Wang, Q. Zhang, L. Wang, X.-W. Yang, *physica status solidi (a)*. **2019**, *216*, 1900228.

[21] S. Huang, L. Duan, D. Zhang, *Journal of Materials Chemistry A*. **2020**, *8*, 18792.

[22] S. Sahi, W. Chen, K. Jiang, *Journal of Luminescence*. **2015**, *159*, 105.

[23] D. Barreca, A. Gasparotto, C. Maccato, C. Maragno, E. Tondello, *Surface Science Spectra*. **2006**, *13*, 87.

[24] B. Han, S. Yu, D. Zhao, Y. Lou, J. Gao, Z. Liu, Z. Wang, G. Qian, *RSC Advances*. **2020**, *10*, 38798.

[25] X. Yu, S. Kato, H. Ito, S. Ono, M. Kase, M. Cadatal-Raduban, *AIP Advances*. **2020**, *10*, 045309.

[26] C. G. Olson, M. Piacentini, D. W. Lynch, *Physical Review B*. **1978**, *18*, 5740.

[27] D. K. Schroder, D. L. Meier, *IEEE Transactions on Electron Devices*. **1984**, *31*, 637.

[28] H. C. Card, *IEEE Transactions on Electron Devices*. **1976**, *23*, 538.

[29] L. G. Gerling, C. Voz, R. Alcubilla, J. Puigdollers, *Journal of Materials Research*. **2017**, *32*.260

[30] H. Nasser, F. Es, M. Zolfaghari Borra, E. Semiz, G. Kökbudak, E. Orhan, R. Turan, *Progress in Photovoltaics: Research and Applications*. **2020**, *29*, 281.

Table of Contents (ToC)

ToC text:

Cerous Fluoride (CeF_3) Dopant-Free electron-selective contacts is fabricated by thermally evaporated in a low temperature process. The Ohmic contact has been formed between n-Si and Al by inserting a 1.5 nm CeF_3 layer, and the contact resistance is about 10.96 $m\Omega \cdot cm^2$. Champion efficiency of 21.27% low-temperature-processed dopant-free n-Si crystalline solar cells have been demonstrated with CeF3/Al stack layer.

ToC figure: